Novel Reclosing Strategy Based on Transient Operating Voltage in Pseudobipolar DC System With Mechanical DCCB

Weijie Wen, *Member, IEEE*, Haijin Liu, Bin Li, *Member, IEEE*, Pengyu Li, Ning Zhang, Chong Gao, and Chengshan Wang, *Senior Member, IEEE*

***Abstract*—To ensure the reliability and flexibility of direct current (dc) system, direct current circuit breakers (DCCBs) are in urgent demand. Compared with solid-state and hybrid DCCBs, mechanical DCCBs have features of low operating losses and investment, showing bright application prospects. Until now, without concern about transient operating voltages (TOV) in the whole dc system, the reclosing of DCCB is still an open problem, and it is the emphasis of this article. First, overview of TOV in typical pseudobipolar dc system is introduced. Then, focused on hardware, electrical characteristic of a novel mechanical DCCB is analyzed, and verification tests are carried out in our laboratory. By taking interaction between the dc system, DCCB, and lines into consideration, distribution patterns of TOV under different faults and its mechanism are revealed. Based on TOV, novel reclosing strategy is proposed for mechanical DCCBs, and case studies are conducted in PSCAD/EMTDC for verification. Remarkable advantages of novel reclosing strategy are: fault type could be identified without operating any component of DCCB after fault current interruption; no risk of reclosing a permanent fault point; an explicit time could be reserved for the dielectric recovery of temporary fault point.**

***Index Terms*—DC circuit breaker, transient operating voltage (TOV), fault-type identification, reclosing.**

I. Introduction

With features of few power conversion steps and high controllability, modular multilevel converters (MMCs) based dc technology is widely recognized as a promising solution to improve the power conversion efficiency and power quality [1]–[2], and large-scale integration of renewable resources. Referring to demonstration projects, such as Nanao (±160 kV) [3] and Zhoushan project (±200 kV) [4], pseudobipolar structure without real ground point at dc side is widely adopted. However, dealing with dc faults is one of the technical difficulties remaining to be overcome.

Compared with using alternating current circuit breakers (ACCB) or converters with dc fault ride-through ability [5], advantages of using direct current circuit breakers (DCCBs) [6]–[8] to deal with dc faults are: 1) transitory blackout of healthy area could be avoided; 2) system operating mode could be adjusted flexibly by using DCCB to switch load current; and 3) DCCB with reclosing capability could deal with permanent and temporary faults differently, meaning stability and reliability of power system are enhanced. Therefore, DCCBs with reclosing capability have great application prospects in the dc system.

Without numerous insulated gate bipolar translators (IGBTs) [9]–[13], mechanical DCCB has remarkable features of negligible operating losses and low investment [14]–[16], and its basic structure is illustrated in Fig. 1.

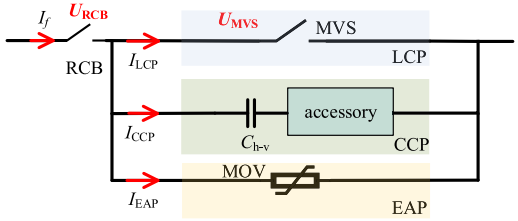

Fig. 1. Basic structure of the mechanical DCCB.

As shown in Fig. 1, mechanical DCCB consists of a residual current breaker (RCB) and three parallel paths including load current path (LCP), current commutation path (CCP), and energy absorption path (EAP). LCP is made of mechanical vacuum switch (MVS). CCP is made of a high-voltage capacitor ($C_{h\text{-}v}$) in series with the accessory for current commutation. The accessory is different when using different current commutation methods, and details could be found in [17]. EAP is made of metal oxide varistor (MOV). In fact, RCB and MVS are ultrafast vacuum mechanical switches, and they could interrupt alternating current with amplitude of tens of kiloampere or direct current with amplitude lower than its chopping current (several Amperes) [18].

Previous research works were focused on current interruption of mechanical DCCB, and rare research is carried out on

Manuscript received January 29, 2020; revised August 4, 2020; accepted September 2, 2020. Date of publication September 7, 2020; date of current version November 20, 2020. This work was supported in part by the State Key Laboratory of Advanced Power Transmission Technology under Grant GEIRI-SKL-2019-001 and in part by the National Natural Science Foundation of China under Grant 51907141. Recommended for publication by Associate Editor F. W. Fuchs. *(Corresponding authors: Haijin Liu; Bin Li.)*

Weijie Wen, Haijin Liu, Bin Li, Pengyu Li, and Chengshan Wang are with the Key Laboratory of Smart Grid of Ministry of Education, Tianjin University, Tianjin 300072, China (e-mail: weijie.wen@tju.edu.cn; liuhaijin@tju.edu.cn; binli@tju.edu.cn; lipengyu1012@163.com; cswang@tju.edu.cn).

Ning Zhang and Chong Gao are with the Global Energy Interconnection Research Institute Co. Ltd, State Grid, Beijing 10084, China (e-mail: shuyening@163.com; gaochong@geiri.sgcc.com.cn).

Color versions of one or more of the figures in this article are available online at https://ieeexplore.ieee.org.

Digital Object Identifier 10.1109/TPEL.2020.3022070

reclosing of mechanical DCCB. Without concern of transient operating voltages (TOV) in the whole power system, two reclosing strategies have been proposed for ACCB and hybrid DCCB, respectively. However, they are not suitable for mechanical DCCBs, and reasons are explained as follows.

Referring to ACCB, one reclosing strategy is to reclose RCB and MVS without identifying fault type (permanent or temporary). When reclosing to permanent fault, secondary surge current is generated, and it has same characteristics with fault current. This reclosing strategy has two fatal shortcomings. First, the two successive surge current might cause unrecoverable damages to vulnerable IGBTs whose surge-handling capability is much lower than conventional electrical devices in ac system [19]. Second, different from ACCB, it is much more difficult for mechanical DCCBs to interrupt surge currents without zero-crossing points twice successively within hundreds of milliseconds [14]–[16].

Referring to hybrid DCCB, the other reclosing strategy [19]–[20] is to reclose RCB only, resulting in CCP parallel with EAP is switched into dc system without producing surge current. Then, based on current and voltage distribution patterns after reclosing RCB, fault type is identified. For permanent faults, RCB is opened again to isolate fault point permanently. For temporary faults, MVS is further reclosed to recover this transmission line. The reclosing strategy requires RCB capable of completing action sequence of open-close-open (O-C-O) within hundreds of milliseconds. However, RCB is actually an ultrafast mechanical switch with mechanical life of 2000–5000, frequent O-C-O operation for RCB is quite difficult [21]. More importantly, decided by random transient voltages distribution pattern on faulty line and hybrid DCCB, fault type identification method for hybrid DCCB is not valid for the mechanical DCCB [19].

Contribution of this article is to propose a novel reclosing strategy for mechanical DCCB based on the characteristic of TOV in the pseudobipolar dc system. The advantage of this reclosing strategy is that the fault type could be identified without operating any component of DCCB after current interruption, meaning no risk of secondary surge current and no requirements for O-C-O of RCB. The rest of article is organized as follows. The overview of TOV is presented in Section II. Focused on hardware, electrical characteristic, and experimental verification of novel mechanical DCCB are presented in Section III. Then, characteristic of TOV under different fault types and its mechanism are revealed in Section IV. Based on the characteristic of TOV, novel reclosing strategy for mechanical DCCBs is proposed is Section V and cases studies are conducted for verification in Section VI. Finally, Section VII concludes this article.

II. Overview of TOV in the Pseudobipolar DC System

Similar with the dc system, when operating DCCBs to isolate faulty line in a pseudobipolar dc system, transient voltage varies with time and space in the whole dc system, and it is defined as TOV in this article. Overview of TOV in the pseudobipolar dc system is introduced as follows.

Considering DCCBs are usually used in multiterminal dc system, diagram of a three-terminal pseudobipolar dc system

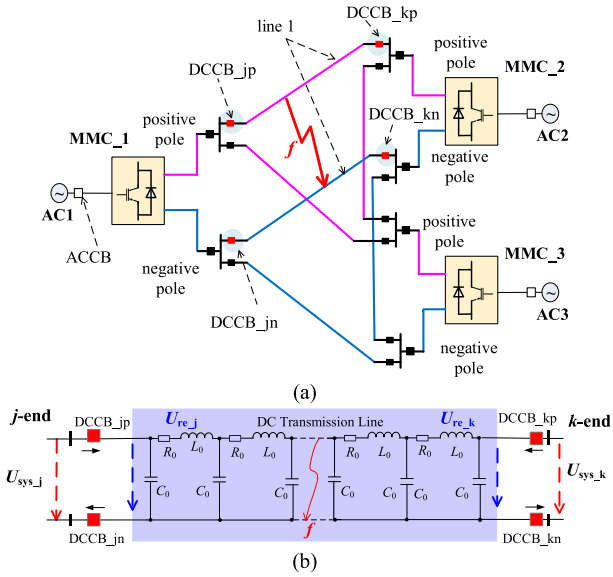

Fig. 2. Pseudobipolar dc system with mechanical DCCBs. (a) Configuration of DCCBs in a typical three-terminal dc system. (b) Distribution of TOV generated by isolating a faulty line with four DCCBs.

with mechanical DCCBs is illustrated in Fig. 2. Because TOV could be generated by operating DCCBs on any lines, line 1 in Fig. 2(a) is taken as an example to introduce TOV, and the diagram of line1 is illustrated in Fig. 2(b). As shown in Fig. 2, *j*-end and *k*-end indicate two ends of the dc transmission line. In a pseudobipolar dc system without real ground point, the transmission line consists of a positive pole and a negative pole. Four DCCBs are installed at each end of each pole of this transmission line.

During the normal state, with DCCBs closed, voltage drop of DCCB is almost zero. Voltage of whole system is rating voltage, and only a small voltage deviation ($\pm 5\% \sim \pm 10\%$) is caused by line losses. Once a fault occurs to line 1, such as $\boldsymbol{f}$ in Fig. 2, four DCCB on this line are triggered to force current through each DCCB to pass through zero, so that the faulty line could be isolated from healthy areas. After complete isolation of faulty line, voltages of healthy areas ($U_{\mathrm{sys\_j}}$, $U_{\mathrm{sys\_k}}$) recover to rating voltage. Residual voltage on faulty line ($U_{\mathrm{res\_j}}$ and $U_{\mathrm{res\_k}}$) is function of time (t) and distance (x). It should be noted, characteristic of residual voltage on faulty line is closely related with fault type, and details are presented in Section IV. Constrained by Kirchhoff's voltage law, voltage on DCCBs (U_{DCCB}) on each pole at each end, equal to voltages on RCB and MVS ($U_{\mathrm{RCB}} + U_{\mathrm{MVS}}$), is half of ($U_{\mathrm{sys\_j}} - U_{\mathrm{res\_j}}$) and ($U_{\mathrm{sys\_k}} - U_{\mathrm{res\_k}}$), respectively.

III. Electrical Characteristic of the Mechanical DCCB With NVS

In theory, fault type (permanent or temporary) could make a difference on TOV in pseudobipolar with mechanical DCCBs, and it could be identified based on this difference. To reveal this difference, electrical characteristics of DCCB are discussed in this part.

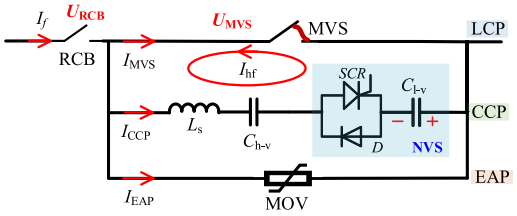

Fig. 3. Mechanical DCCB with NVS.

A. Structure of Mechanical DCCB With NVS

According to [17], for existing mechanical DCCBs with active current commutation methods, precharged capacitor is essential for the accessory in CCP, and high voltage (tens or even hundreds of kilovolts) will be applied on this capacitor, meaning electrical insulation requirements for this capacitor and its charging system is so high that it is one of main technical difficulties for mechanical DCCB. To solve this problem, a negative voltage source (NVS) proposed by us is deployed in mechanical DCCB for current commutation, and its structure is illustrated in Fig. 3.

As shown in Fig. 3, the novel mechanical DCCB with NVS consists of RCB and three parallel paths, including LCP, CCP, and EAP. NVS is made of a low-voltage capacitor ($C_{\text{l-v}}$) and thyristor (SCR) antiparalleled with diode (D). L_{s} is intrinsic stray inductance of loop-circuit made of LCP and CCP, and it is usually several microhenry.

It should be noted, $C_{\text{h-v}}$ is in series with $C_{\text{l-v}}$, just like a capacitive voltage divider. When SCR is turned ON, voltage variation ratio of $C_{\text{h-v}}$ and $C_{\text{l-v}}$ is equal to capacitance ratio of $C_{\text{l-v}}$ and $C_{\text{h-v}}$. Referring to existing mechanical DCCBs, capacitance of $C_{\text{h-v}}$ is in the range of 10–60 μF, and the maximum voltage variation of $C_{\text{h-v}}$ is $\sim$2 p.u., which is decided by the clamping voltage of MOV. Therefore, as long as capacitance of $C_{\text{l-v}}$ is large enough, voltage variation of $C_{\text{l-v}}$ could be only several kilovolts, meaning electrical insulation requirements for NVS and its charging system could be reduced dramatically.

B. Working Principle of Mechanical DCCB With NVS

In the pseudobipolar dc system shown in Fig. 2(b), during the normal state, RCB and MVS in all mechanical DCCBs are closed. $C_{\text{l-v}}$ in NVS is precharged with several kilovolts. SCR in NVS is turned OFF. In this case, precharged voltage on $C_{\text{l-v}}$ is blocked by SCR antiparallel with D, and initial voltage on $C_{\text{h-v}}$ is zero. Load current flows through RCB in series with MVS. Voltage on DCCB(U_{DCCB}) is almost zero, and voltage of the whole system is rating voltage.

Considering the most severe working condition of pole-to-pole short-circuit fault, just as shown in Fig. 2, all converters at *j*-end and *k*-end provide fault currents ($I_{\text{f\_j}}$, $I_{\text{f\_k}}$) to the fault point (I_{f}). Two mechanical DCCBs (DCCB_jp and DCCB_jn) at *j*-end are triggered together to interrupt $I_{\text{f\_j}}$ provided by the dc system at *j*-end. Similarly, two mechanical DCCBs (DCCB_kp and DCCB_kn) at *k*-end are also triggered together to interrupt $I_{\text{f\_k}}$. As a result, faulty line is isolated from healthy area.

Taking DCCB_jp and DCCB_jn as an example, current interruption process of $I_{\text{f\_j}}$ is described as follows: MVS and RCB are commanded to open first. After time delay of $\sim$2 ms for the establishment of contacts distance, SCR in NVS is turned ON. With initial voltages on $C_{\text{h-v}}$ and $C_{\text{l-v}}$ not equal, the turn-ON of SCR ignites an oscillatory current with high-frequency (I_{hf}) in the loop circuit with LCP and CCP in series, just as shown in Fig. 3. As long as the amplitude of I_{hf} is larger than fault current ($I_{\text{f\_j}}$), current through MVS (I_{MVS}) will pass through zero, resulting in MVS extinguished and $I_{\text{f\_j}}$ completely commutated CCP(I_{CCP}). Then, caused by the interaction between healthy area, CCP parallel with EAP, and faulty line, transient interruption voltage is established on DCCB_jp and DCCB_jn to force $I_{\text{f\_j}}$ to zero. Finally, RCB is extinguished at zero-crossing point of $I_{\text{f\_j}}$, resulting in the differential voltage between healthy area and faulty line is completely applied on RCB (U_{RCB}) and MVS (U_{MVS}) in DCCB.

It should be noted, with the existence of faulty point, TOV at one end of faulty line, such as $U_{\text{sys\_j}}$, $U_{\text{res\_j}}$, U_{DCCB} at *j*-end, is generated by the interaction between power system, two DCCBs and faulty line at this end, and it is not related with the other end. However, when the faulty point disappears, TOV at both end will be affected by each other. Further details will be presented in Sections IV and V.

C. Experiments on Prototype of Mechanical DCCB With NVS

To verify the mechanical DCCB with NVS, a prototype with rating voltage of 2 kV has been established in our laboratory. Just as shown in Fig. 4(a), typical current interruption experimental circuits for DCCBs [15]–[17], [20] are used. C_{DC} (40 mF) in series with L_{DC} (1mH) is equivalent to the dc system consisting of MMCs. The picture of prototype and experimental platform is shown in Fig. 4(b), and experimental results are illustrated in Fig. 4(c).

Parameters of the prototype are listed as follows: Ls is $\sim$6 μH; knee voltage, clamping voltage, and energy capacity of MOV are 2 kV, $\sim$3 kV, and 20 MJ; $C_{\text{h-v}}$ is 140 μF; $C_{\text{l-v}}$ is 520 μH; precharged voltage on $C_{\text{h-v}}$ is zero; precharged voltage on $C_{\text{l-v}}$ is 0.5 kV, and its direction is shown in Fig. 4(a).

Before the test, RCB is open, and MVS is closed. SCR is turned OFF. C_{DC} and $C_{\text{l-v}}$ are precharged. The test is ignited by the closing of RCB, and C_{DC} starts discharging through L_{DC} to produce the current to be interrupted. In the test, to observe the first current commutation process, two Rogowski Coils are used to measure the current through LCP (I_{MVS}), and CCP parallel with EAP ($I_{\text{CCP}} + I_{\text{EAP}}$), respectively. In order to observe voltage variation on $C_{\text{h-v}}$ and $C_{\text{l-v}}$, two voltage differential probes are used to measure voltages on MVS (U_{MVS}) and $C_{\text{l-v}}$ (U_{clv}), respectively.

As shown in Fig. 4(c), when current reaches 2.7 kA, MVS is commanded to open at t_0 (0 ms). After time delay for establishment of contacts distance, SCR in NVS is turned ON at t_1 (2 ms), resulting in current commutates from LCP to CCP rapidly. After current commutation from LCP to CCP driven by NVS, I_{CCP} charges $C_{\text{h-v}}$ in series with $C_{\text{l-v}}$ continuously, resulting in U_{MVS} increases until it is limited to be clamping voltage of MOV (3.1 kV) and current further commutates to EAP (I_{EAP}) naturally. Then, with U_{MVS} larger than voltage on C_{DC},

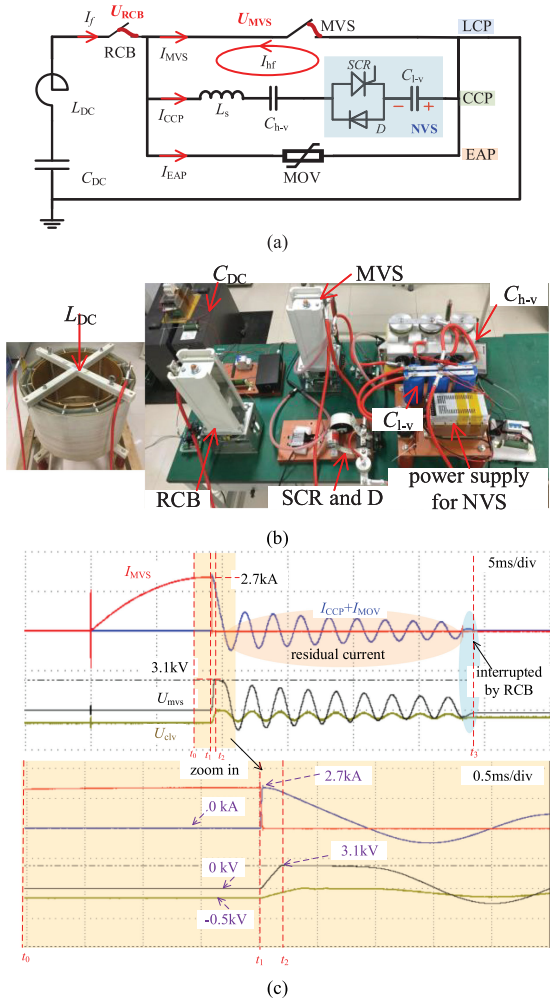

Fig. 4. Test circuit and photographs of the experiment platform and prototype. (a) Test circuit for prototype. (b) Photographs of the experiment platform and prototype. (c) Experimental results.

I_f (equal to I_{EAP} during this period) starts decreasing. Decided by volt-ampere characteristic of MOV, with I_{EAP} decreasing, U_{MVS} which is actually the voltage on MOV also decreases until MOV turns back into high-resistance state, resulting in current commutates back to CCP. Finally, because this residual current has natural zero-crossing points, it can be easily interrupted by opening RCB at t_3. In tests, t_3 is set to be 20 ms so that RCB could extinguish later and the alternating residual current could be observed clearly.

Without loss of generality, test results of prototype with low rating voltage and current have verified the effectiveness of mechanical DCCB with NVS, and dc with amplitude of ~2.7 kA could be forced to decrease within 2 ms.

IV. Characteristic of TOV in the Pseudobipolar DC System

In this section, focused on the interaction between power system, mechanical DCCB, and faulty line, characteristic of TOV in the dc system under different fault types is studied in this part.

TABLE I
Parameters of Simulation Models

Item	MMC_1	MMC_2	MMC_3
Rated power/MW	400	200	200
Rated DC voltage /kV	±200	±200	±200
Number of sub-modules in each bridge arm	100	100	100
Capacitance of sub-modules /μF	13000	9750	9750
Reactance of bridge arm/mH	19.1	37.6	37.6
Current limiter/mH	50	50	50

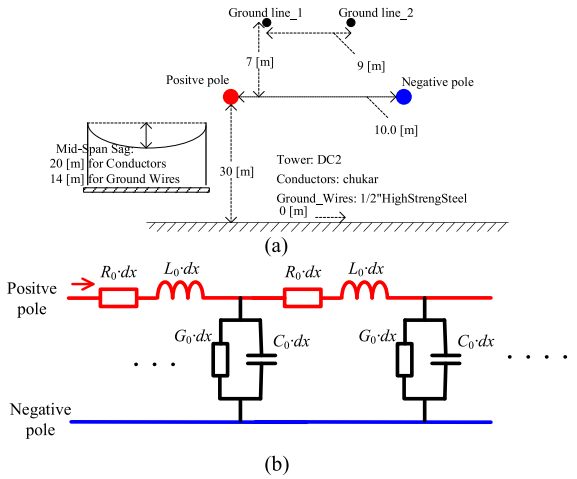

Fig. 5. Structure of the transmission line and its detailed distributed parameter model. (a) Physical dimension of transmission lines. (b) Detailed distributed parameter model of transmission lines.

A. Simulation Model

Referring to the three-terminal dc system with novel mechanical DCCBs in Fig. 2, simulation model of the pseudobipolar dc system with overhead lines is established in PSCASD/EMTDC.

1) Parameters of MMCs: In the simulation, the pseudobipolar dc system with rating voltage of ±200 kV consists of three MMCs, and detailed parameters of MMCs could be found in Table I.

2) Parameters of overhead lines: Considering that faults probability of overhead line is quite high, and it poses main demands for the reclosing of DCCB, overhead lines are used as power transmission carrier in the simulation, and length of all three lines connecting MMC_1, MMC_2, and MMC_3 is equal to 200 km. The detailed physical dimensions of the overhead lines are illustrated in Fig. 5(a), and its distributed parameter model is shown in Fig. 5(b). In the simulation, frequency-dependent line model with high precision is adopted, and the characteristic of R0 and L0 varying with frequency has been considered.

3) Parameters of mechanical DCCB with NVS: In the simulation, 18 mechanical DCCBs with NVS are installed, and detailed parameters of DCCB are listed as follows: L_s is ~10 μH; $C_{h\text{-}v}$ is 20 μF; $C_{l\text{-}v}$ is 2000 μH; precharged voltage on $C_{h\text{-}v}$ is zero;

TABLE II
PARAMETERS OF MOV

Current (kA)	0.001	0.01	0.1	0.2	0.38	0.65	1.11	1.50	2.00	2.80	200.0
Voltage (p.u)	1.1	1.6	1.7	1.54	1.78	1.82	1.85	1.88	1.91	1.95	3.2

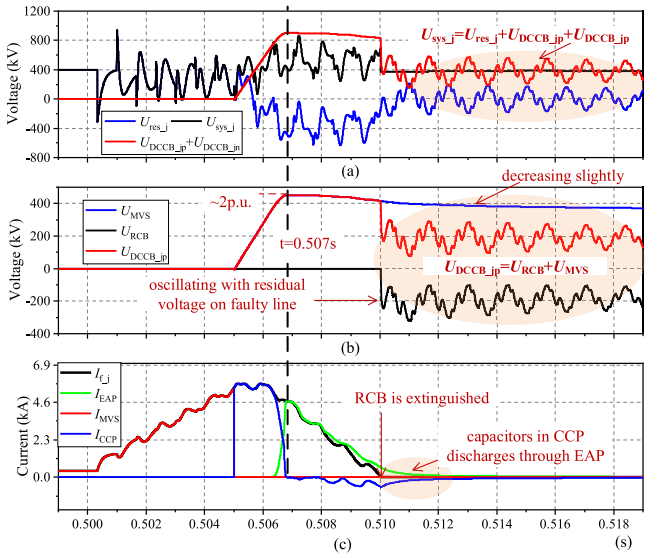

Fig. 6. Detailed voltages and currents inside DCCB_jp under permanent faults. (a) Transient voltages at *j*-end. (b) Transient voltages inside DCCB_jp. (c) Current inside DCCB_jp.

precharged voltage on $C_{l\text{-}v}$ is 10 kV. Volt-Ampere parameters of MOV are listed in Table II.

It should be noted that MOV is designed in accordance of system parameters. In simulations, to ensure successful interruption of fault current with small amplitude, rating voltage of MOV is set to be 200 × 1.15 kV, so that leaking current of MOV under rating system voltage (200 kV) is lower than chopping current of RCB (several Amperes).

B. Discussion on TOV Under Permanent Faults

Referring to Fig. 2(a), a typical permanent pole-to-pole short-circuit fault occurs at the middle of line 1 at 0.5 s. After 3 ms for protection relay, four mechanical DCCBs in Fig. 2(b) are triggered, meaning RCB and MVS are commanded to open at 0.503 s. Then, after 2 ms for contacts separation in MVS and RCB, SCR is turned ON at 0.505 s. Taking DCCB_jp in Fig. 2(b) as an example, detailed voltages and current inside DCCB under permanent fault are illustrated in Fig. 6.

Before 0.505 s, I_{f_j} is completely conducted by MVS in LCP (I_{MVS}). Then, current commutates from LCP (I_{MVS}) to CCP (I_{CCP}) driven by the turn-ON of SCR at 0.505 s. Caused by the charging effect of capacitors ($C_{h\text{-}v}$ in series with $C_{l\text{-}v}$) by I_{CCP}, U_{MVS} increases until it is limited to be clamping voltage of MOV (~2 p.u.), resulting in current further commutates from CCP (I_{CCP}) to EAP (I_{EAP}) at ~0.507 s. After 0.507 s, with U_{DCCB} (~2 p.u.) larger than system rating voltage, I_{f_j} is forced to pass through zero and finally interrupted by RCB at 0.51 s.

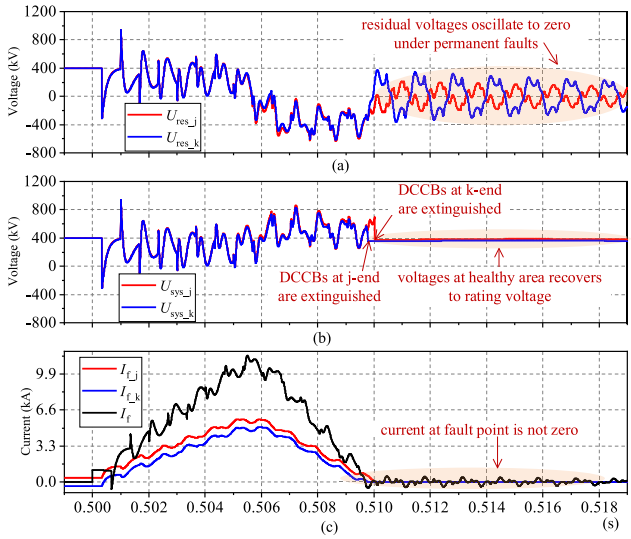

Fig. 7. System voltages and current at *j*-end and *k*-end under permanent faults. (a) Residual voltage on faulty line. (b) Voltages of healthy area. (c) Fault current.

During 0.505–0.51 s, I_{f_j} has not pass through zero and RCB is arcing, voltage on DCCB (U_{DCCB}) is equal to U_{MVS}, just as shown in Fig. 6(b). During 0.507–0.51 s, decided by the volt-ampere characteristic of MOV U_{DCCB} equal to voltage on MOV, decreases slightly with I_{f_j}, and equivalent resistance of MOV increases. During this period, capacitors discharge through EAP slightly, resulting in a small fraction of current flows through CCP, just as shown in Fig. 6(c).

After 0.51 s when DCCB is completely extinguished, U_{MVS} decreases slightly as shown in Fig. 6(b); voltage of healthy area (U_{sys_j}) recovers to be rating voltage (400 kV); voltages on DCCBs (U_{DCCB_jp} and U_{DCCB_jn}) oscillates with residual voltage of faulty line at j-end (U_{res_j}) significantly. In fact, before DCCBs are extinguished, U_{sys_j} also oscillates with U_{res_j}. To further observe the oscillating phenomena of TOV clearly, system voltages and current at both *j*-end and *k*-end under permanent fault are illustrated in Fig. 7.

As shown in Fig. 7, DCCBs at *j*-end and *k*-end are extinguished when I_{f_j} and I_{f_k} passes through zero at different time, resulting in faulty line is completely isolated. Voltages of healthy areas (U_{sys_j}, U_{sys_k}) at *j*-end and *k*-end recover to rating voltage (400 kV). After faulty line is isolated, U_{res_j} and U_{res_k} still oscillate continuously, and they have different shapes and amplitudes; along with U_{res_j} and U_{res_k}, I_f also oscillates, just as shown in Fig. 7(c).

The reasons are explained as follows. The equivalent circuit of faulty line isolated by four DCCBs is illustrated in Fig. 8. After 0.510 s, because MVS is parallel with equivalent capacitors in CCP, U_{MVS} cannot change suddenly. With capacitors in CCP discharging through MOV by leaking current of several amperes in Fig. 6(c), U_{MVS} decreases slightly, just as shown in Fig. 6(b).

During the normal state (before 0.5 s), voltage in the whole system is almost equal to the rating voltage. Once a fault occurs at 0.5 s, shunt capacitance (C_0) will discharge through serial resistance (R_0) and serial inductance (L_0) to fault point. With

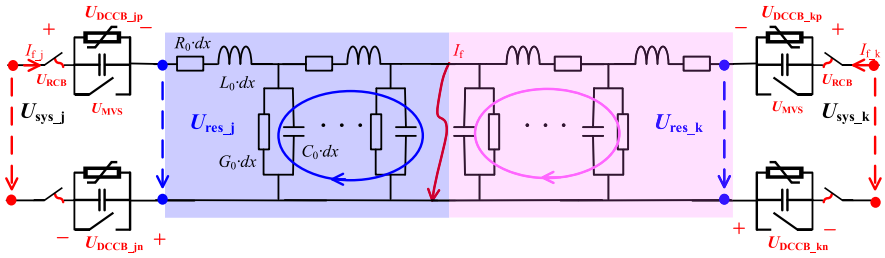

Fig. 8. Equivalent circuit of the isolated faulty line with four DCCBs in the pseudobipolar dc system.

numerous C_0 discharging through R_0 and L_0 of line with different length to the fault point, transient current and voltage waves with multiple frequency components are produced, resulting in $I_{\mathrm{f\_j}}$ and $U_{\mathrm{res\_j}}$ oscillates significantly. Before 0.51 s, DCCB has not been extinguished, oscillating current and voltage wave could travel across DCCB to the healthy area, resulting in $U_{\mathrm{sys\_j}}$ also oscillates with $U_{\mathrm{res\_j}}$. After 0.51 s, DCCB is extinguished, oscillatory current wave will be completely reflected back to fault point, and transient voltage wave only travels along the isolated faulty line. Thus, when both $I_{\mathrm{f\_j}}$ and $I_{\mathrm{f\_k}}$ are completely extinguished, I_{f} still exists because of the oscillation between C_0, R_0, and L_0 in Fig. 8.

According to Kirchhoff's voltage law, $U_{\mathrm{DCCB}} = U_{\mathrm{RCB}} + U_{\mathrm{MVS}}$ and $U_{\mathrm{sys\_j}} = U_{\mathrm{res\_j}} + U_{\mathrm{DCCB\_jp}} + U_{\mathrm{DCCB\_jn}}$. As mentioned before, with faulty line isolated, $U_{\mathrm{sys\_j}}$ recovers to rating voltage. Clamped by capacitors (in the order of μF) in CCP, U_{MVS} only decreases slightly. With stray capacitance of RCB in the order of pF, U_{RCB} could change suddenly with $U_{\mathrm{res\_j}}$, resulting in U_{RCB} and U_{DCCB} oscillate with $U_{\mathrm{res\_j}}$ significantly.

Clearly, if the fault point is permanent, all C_0 will discharge to the fault point until residual voltages on the faulty line at *j*-end ($U_{\mathrm{res\_j}}$) reach zero. Similarly, $U_{\mathrm{res\_k}}$ also oscillates to zero. However, as shown in Fig. 8, the faulty line is split into two segments, and transient current and voltage wave at *j*-end cannot travel to *k*-end, resulting in $U_{\mathrm{res\_j}}$ and $U_{\mathrm{res\_k}}$ have different shapes and amplitudes, just as shown in Fig. 7(a). Both $U_{\mathrm{res\_j}}$ and $U_{\mathrm{res\_k}}$ will decay to zero until all energy stored in C_0 of the two segments is dissipated, respectively.

C. Discussion on TOV Under Temporary Faults

For temporary fault, a pole-to-pole fault also occurs at the middle of line 1 at 0.5 s. DCCBs are triggered at 0.503 s. SCR is turned ON at 0.505 s. Considering that arc at the fault point might be extinguished at zero-crossing point of I_f and dielectric insulation strength could recover, the duration time of fault is set to be 20 ms, and the fault point disappears at 0.52 s. Because transient current and voltages inside DCCB under permanent and temporary faults are similar, only transient current and voltages in power system are illustrated in Fig. 9.

Comparing Figs. 7 and 9, before 5.2 s when the fault point disappears, characteristics of transient current and voltage distribution patterns under temporary fault are similar with permanent fault. Current at the fault point is extinguished at 0.52 s. A very interesting phenomenon is that after 5.2 s when fault point

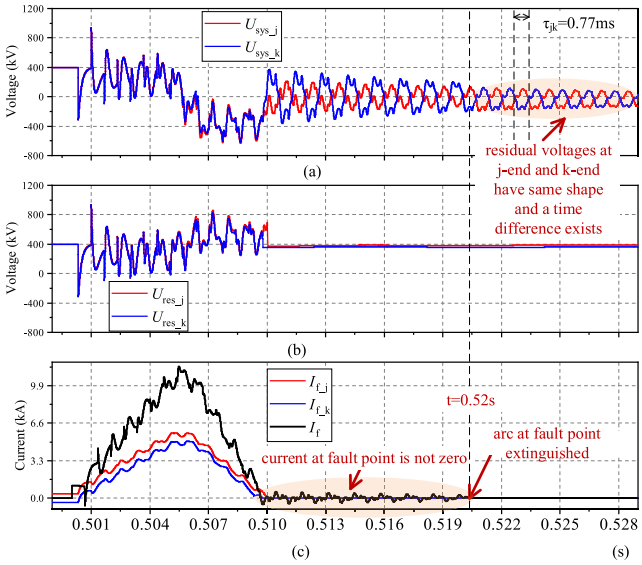

Fig. 9. System voltages and current at both *j*-end and *k*-end under temporary faults. (a) Residual voltage on faulty line. (b) Voltages of healthy area. (c) Fault current.

disappears, residual voltages on the faulty line at *j*-end and *k*-end have same shape and amplitude, and only a time difference of 0.77 ms exists, just as shown in Fig. 9(a). The reasons are explained as follows.

Referring to distributed parameter model of transmission line in Fig. 5(b), as long as there is no fault point on the transmission line between *j*-end and *k*-end, by neglecting resistance and conductance, current and voltage along this transmission line is function of time (t) and distance (x), just as given in the following equation:

$$\begin{cases} \dfrac{\mathrm{d}u_0(x,t)}{dx} = -\left(L_0 \dfrac{di_0(x,t)}{dt}\right) \\ \dfrac{\mathrm{d}i_0(x,t)}{dx} = -\left(C_0 \dfrac{du_0(x,t)}{dt}\right). \end{cases} \tag{1}$$

Before 5.2 s, the fault point is actually a breakpoint of the transmission line, and transient voltage waves ($U_{\mathrm{res\_j}}$) at j-end will be reflected back at the fault point. Especially, when the fault is metallic with zero-impedance, negative total reflection of transient voltage waves occurs at the fault point, meaning $U_{\mathrm{res\_j}}$ cannot travel across fault point to j-end, and $U_{\mathrm{res\_j}}$ has different shape and amplitude with $U_{\mathrm{res\_k}}$.

After 0.52 s when the fault point disappears, referring to (1), transient voltage travels along the isolated line, and positive total

reflection of transient voltage waves occur at *j*-end and *k*-end, respectively, meaning with all four DCCB completely open and no fault point, residual voltages of the faulty line at *j*-end and *k*-end have same shape and only a time difference of $\tau_{\rm jk}$ exists. $\tau_{\rm jk}$ is the time for transient voltage waves traveling from *j*-end to *k*-end, and it is decided by line length and travelling speed of transient voltage wave. In the simulation case, with length of ~200 km and travelling speed of ~300 km/ms, $\tau_{\rm jk}$ is ~0.77 ms, just consistent with Fig. 9(c).

V. Novel Reclosing Strategy Based on Differential Residual Voltages on Faulty Line

Characteristics of TOV are quite different under permanent and temporary faults. Based on this difference, a novel reclosing strategy for mechanical DCCB, in which fault type could be identified in advance, is proposed in this section.

A. Fault Type Identification Based on Residual Voltages

According to the theoretical analysis in Sections IV-B and IV-C, after faulty line is isolated from healthy area, residual energy stored by C_0 of transmission line dissipates through the fault point until arc at the fault point extinguishes, resulting in oscillation between C_0, L_0, and R_0, and oscillatory residual voltage at *j*-end and *k*-end. Under permanent fault, the transmission line is divided into two segments by the fault point, $U_{\rm res\_j}$ and $U_{\rm res\_k}$ have different shape and amplitude, and they decay to zero at different time. Under temporary fault, after the fault point disappears, transient voltage wave travel along the line successively, and be reflected back completely at each end, resulting in $U_{\rm res\_j}$ and $U_{\rm res\_k}$ have same shape and amplitude, and only a time difference for wave travelling exists. Based on this difference, a fault-type identification method based on differential residual voltages is constructed, just as shown in (2).

$U_{\rm res\_j}$ and $U_{\rm res\_k}$ are measured signals at *j*-end and *k*-end of the isolated transmission line. $\tau_{\rm jk}$ is the time difference for voltage waves travelling from *j*-end to *k*-end, and it is the ratio of whole length of the transmission line ($l_{\rm jk}$) and propagation speed of voltage wave ($v_{\rm jk}$). *S* is the threshold value to ensure correctness of fault-type identification. Usually, 0.1 is enough for *S*

$$\begin{aligned}&\text{if } \left(|U_{res\_j}(t)|+|U_{res\_j}(t)|\neq 0\right)\\&\quad\text{and } \left(T=\frac{|U_{res\_j}(t)-U_{res\_k}(t-\tau_{jk})|}{|U_{res\_j}(t)|+|U_{res\_j}(t)|}<S\right)\\&\qquad F{=}1\\&\quad\text{else}\\&\qquad F=0.\end{aligned}\tag{2}$$

After DCCBs are completely open and fault point disappears, $U_{\rm res\_j}(t)$ is almost equal to $U_{\rm res\_k}(t-\tau_{\rm jk})$; $T\approx 0<\mathrm{S}=0.1$, and *F* is 1. In this case, the fault is identified as temporary fault. Otherwise, the fault point always exists; $U_{\rm res\_j}$ is not equal to $U_{\rm res\_k}$, *T* is not 0 and *F* is 0. In this case, the fault is identified as permanent fault.

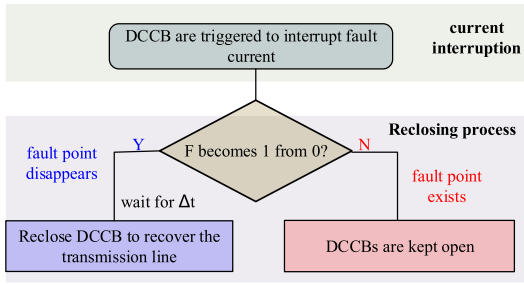

Fig. 10. Novel reclosing strategy for DC-CB.

B. Novel Reclosing Strategy With Fault-Type Identification

Based on the fault-type identification in (2), the novel reclosing strategy for mechanical DCCB with NVS is illustrated in Fig. 10. Before DCCBs are triggered, *F* is set to be 1, indicating no fault along the transmission line. After DCCB are triggered to interrupt fault current, *F* is obtained by (2). *F* is 0 when the fault occurs, and it becomes 1 from 0 when arc at the fault point extinguishes. In this situation, an explicit time delay (Δt) of ~100 ms is reserved for dielectric strength recovery at the faulty point. Then, DCCBs are reclosed, and *F* becomes 1 after DCCBs are closed. If *F* is always 0 after the fault occurrence, the fault is identified as permanent fault. In this situation, no more operating of DCCB is needed, and the faulty line is isolated from the healthy area permanently.

It should be noted, in the novel reclosing strategy, the time when *F* becomes 1 from 0 is the time when arc at the fault point extinguishes. With the exact time when fault point disappears known, an explicit time delay could be reserved for the dielectric recovery of the fault point. However, in existing reclosing strategies for ACCB and hybrid DCCB mentioned in Section I, the time when arc at the fault point disappears is unpredictable. Comparing with the existing reclosing strategies in Section I, advantages of the novel reclosing strategy are as follows: 1) under permanent fault, no secondary surge current is produced and there is no requirement for operating any components of DCCB; 2) under temporary fault, the time when the fault point disappears could be determined, and an explicit time for dielectric recovery of the fault point could be reserved.

VI. Case Study

Based on the simulation model in Section IV, case studies on the novel reclosing strategy are conducted, and they are discussed in this section.

A. Case Study on Reclosing Strategy for Permanent Fault

Similar with Section IV-B, a pole-to-pole permanent short-circuit fault occurs at the middle of line 1 at 0.5 s. DCCBs are triggered to open at 0.503 s. Transient current and voltage, and the faulty-type identification results of dealing with permanent fault are illustrated in Fig. 11.

As shown in Fig. 11(a) and (b), after the fault occurs at 0.5 s, transient voltage and current oscillates until all energy stored by C_0 of transmission line discharges through the fault point

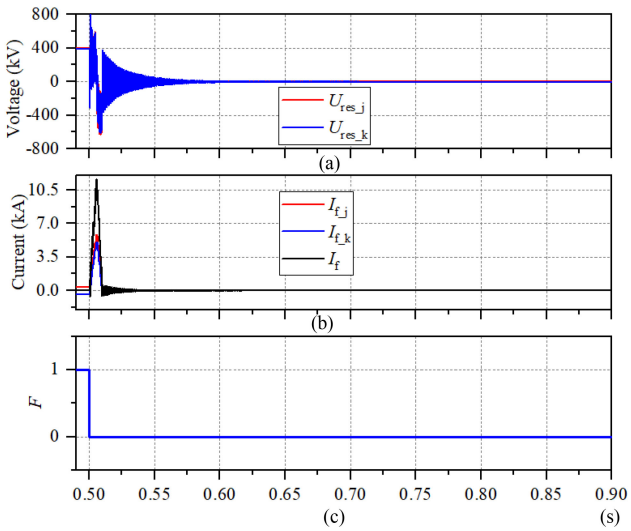

Fig. 11. Transient voltage current and voltage and fault type identification under permanent fault. (a) Voltage. (b) Current. (c) Identification results.

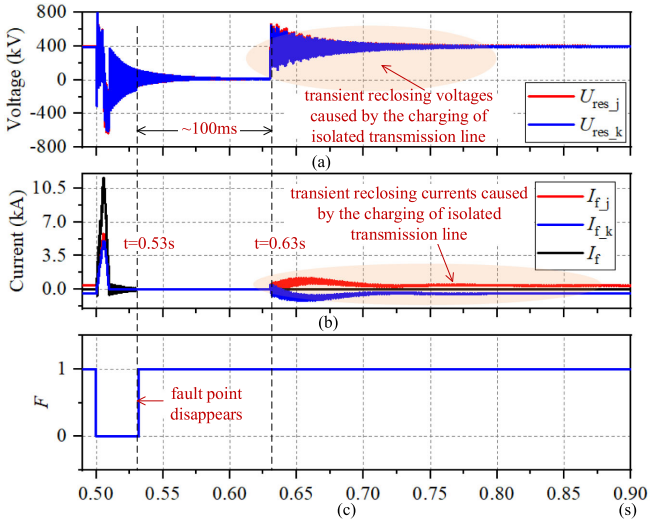

Fig. 12. Transient voltage current and voltage and fault-type identification under temporary fault. (a) Voltage. (b) Current. (c) Identification results.

completely. As shown in Fig. 11(c), F is always 0, meaning the permanent fault could be identified without operating any component in the mechanical DCCB with NVS and no secondary surge current is produced.

B. Case Study on Reclosing Strategy for Temporary Fault

Similar to Section IV-C, a pole-to-pole short-circuit fault occurs at the middle of line 1 at 0.5 s. DCCBs are triggered to open at 0.503 s, and the fault point disappears at 0.53 s. Transient current and voltage, and the faulty-type identification results of dealing with temporary fault are illustrated in Fig. 12.

As shown in Fig. 12(a) and (b), after the fault occurs at 0.5 s, transient voltage and current oscillate along with energy stored by C_0 of the transmission line dissipating through the fault point. After the fault interruption of all DCCBs, current at the fault point extinguishes at 0.53 s when the fault point disappears. As shown in Fig. 11(c), after DCCB are triggered, F is 0 when the fault point exists, and it becomes 1 when the fault point disappears, meaning the time when temporary fault point disappears is recognized when F becomes 1 from 0. Then, after an explicit time delay for dielectric recovery of the fault point, DCCBs are closed to recover this transmission line. Caused by the charging of transmission line, transient current and voltage appear and they could recover to the normal state before this fault.

VII. Conclusion

DCCBs with reclosing capability are essential to ensure the safety and flexibility of dc system based on MMCs. This article is focused on the reclosing of mechanical DCCBs, which is still an open problem. First, overview of transient voltages in the whole dc system generated by operating DCCBs is introduced. Then, focused on hardware, a novel mechanical DCCB is proposed and tests on prototype have verified this mechanical DCCB. By analyzing the interaction between power system, DCCB and lines, characteristics of TOV are revealed: under permanent fault, residual voltages at two ends of the isolated faulty line decay to zero; under temporary fault, residual voltages at two ends of the isolated faulty line have same shape and amplitude after fault point disappears. Based on this characteristic, novel reclosing strategy is proposed for mechanical DCCBs, and case studies for verification are conducted in PSCAD/EMTDC. Research results show that novel reclosing strategy has remarkable advantages: fault type could be identified without operating any component of DCCB after fault current interruption; no risk of reclosing a permanent fault point; the time when the fault point disappears could be detected and an explicit time could be reserved for the dielectric recovery of temporary fault point.

In this article, the fault point is regarded as a discharging gap which extinguishes naturally at zero-crossing point of fault current, just like that in the ac system. However, detailed characteristic of fault point in the dc system should be further studied in real projects. In addition, future studies will be carried out on true bipolar dc system with real grounding point.

References

[1] R. Wang, Q. Sun, X. Liu, and D. Ma, "Power flow calculation based on local controller impedance features for the AC microgrid with distributed generations," *IET Energy Syst. Integration*, vol. 1, no. 3, pp. 202–209, 2019.

[2] M. A. Ebrahim, F. Wadie, and M. A. Abd-Allah, "Integrated fault detection algorithm for transmission, distribution, and microgrid networks," *IET Energy Syst. Integration*, vol. 1, no. 2, pp. 104–113, 2019.

[3] J. Fu, Z. Yuan, Y. Wang, S. Xu, W. Wei, and Y. Luo, "Control strategy of system coordination in Nanao multi-terminal VSC-HVDC project for wind integration," in *Proc. IEEE PES General Meeting Conf. Expo.*, National Harbor, MD, USA, 2014, pp. 1–5.

[4] G. Tang, Z. He, H. Pang, X. Huang, and X. Zhang, "Basic topology and key devices of the five-terminal DC grid," *CSEE J. Power Energy Syst.*, vol. 1, no. 2, pp. 22–35, Jun. 2015.

[5] G. Li, W. Liu, T. Joseph, J. Liang, and Z. Song, "Double-thyristor-based protection for valve-side single-phase-to-ground faults in HB-MMC-based bipolar HVDC systems," *IEEE Trans. Ind. Electron.*, vol. 67, no. 7, pp. 5810–5815, Jul. 2020.

[6] J. Häfner and B. Jacobson, "Proactive hybrid HVDC breakers—A key innovation for reliable HVDC grids," in *Proc. Elect. Power Syst. Future, Integrating Supergrids Microgrids, CIGRE Symp.*, Bologna, Italy, 2011.

[7] W. Xiangguang, G. Chong, L. Xiang, Z. Wandi, and W. Yanan, "A novel design of high-voltage DC circuit breaker in HVDC flexible transmission grid," *Autom. Elect. Power Syst.*, vol. 37, no. 15, pp. 95–102, Aug. 2013, (In Chinese).

[8] C. M. Franck, "HVDC circuit breakers: A review identifying future research needs," *IEEE Trans. Power Del.*, vol. 26, no. C, pp. 998–1007, Apr. 2011.

[9] A. Mokhberdoran, D. Van Hertem, N. Silva, H. Leite, and A. Carvalho, "Multiport hybrid HVDC circuit breaker," *IEEE Trans. Ind. Electron.*, vol. 65, no. 1, pp. 309–320, Jan. 2018.

[10] G. Liu, F. Xu, Z. Xu, Z. Zhang, and G. Tang, "Assembly HVDC breaker for HVDC grids with modular multilevel converters," *IEEE Trans. Power Electron.*, vol. 32, no. 2, pp. 931–941, Feb. 2017.

[11] E. Kontos, T. Schultz, L. Mackay, L. M. Ramirez-Elizondo, C. M. Franck, and P. Bauer, "Multiline breaker for HVdc applications," *IEEE Trans. Power Del.*, vol. 33, no. 3, pp. 1469–1478, Jun. 2018.

[12] X. Pei, O. Cwikowski, A. C. Smith, and M. Barnes, "Design and experimental tests of a superconducting hybrid DC circuit breaker," *IEEE Trans. Appl. Supercond.*, vol. 28, no. 3, Apr. 2018, Art no. 5000205.

[13] X. Zhang, Z. Yu, Z. Chen, B. Zhao, and R. Zeng, "Optimal design of diode-bridge bidirectional solid-state switch using standard recovery diodes for 500-kV high-voltage DC breaker," *IEEE Trans. Power Electron.*, vol. 35, no. 2, pp. 1165–1170, Feb. 2020.

[14] S. Liu *et al.*, "Modeling, experimental validation, and application of VARC HVDC circuit breakers," *IEEE Trans. Power Del.*, vol. 35, no. 3, pp. 1515–1526, Jun. 2020.

[15] Y. Wu, M. Rong, Y. Wu, F. Yang, and Q. Yi, "Damping HVDC circuit breaker with current commutation and limiting integrated," *IEEE Trans. Ind. Electron.*, vol. 67, no. 12, pp. 10433–10441, Dec. 2020.

[16] L. Liu *et al.*, "Design and test of a new kind of coupling mechanical HVDC circuit breaker," *IET Gener., Transmiss. Distrib.*, vol. 13, no. 9, pp. 1555–1562, 2019.

[17] W. Wen, Y. Wang, B. Li, Y. Huang, R. Li, and Q. Wang, "Transient current interruption characteristics of a novel mechanical DC circuit breaker," *IEEE Trans. Power Electron.*, vol. 33, no. 11, pp. 9424–9431, Nov. 2018.

[18] M. Tsukima, J. Abe, H. Kitanaka, and H. Koga, "Vacuum switch chopping current in an inverter circuit," *IEEE Trans. Plasma Sci.*, vol. 39, no. 6, pp. 1364–1369, Jun. 2011.

[19] B. Li, J. He, Y. Li, and W. Wen, "A novel DCCB reclosing strategy for the flexible HVDC grid," *IEEE Trans. Power Del.*, vol. 35, no. 1, pp. 244–257, Feb. 2020.

[20] K. Vinothkumar, I. Segerqvist, N. Johannesson, and A. Hassanpoor, "Sequential auto-reclosing method for hybrid HVDC breaker in VSC HVDC links," in *Proc. IEEE 2nd Annu. Southern Power Electron. Conf.*, Auckland, 2016, pp. 1–6, doi: 10.1109/SPEC.2016.7846120.

[21] W. Wen *et al.*, "Research on operating mechanism for ultra-fast 40.5-kV vacuum switches," *IEEE Trans. Power Del.*, vol. 30, no. 6, pp. 2553–2560, Dec. 2015.

[22] Z. Zhang *et al.*, "Short-circuit current calculation and performance requirement of HVDC breakers for MMC-MTDC systems, " *IEEJ Trans. Elect. Electron. Eng.*, vol. 11, no. 2, pp. 168–177, Mar. 2016.